International Journal of Fluid Machinery and Systems
Vol. 8, No. 3, July-September 2015

DOI: 10.5293/IJFMS.2015.8.3.155
ISSN (Online): 1882-9554

Original Paper

Comparison of steady and unsteady simulation methodologies for predicting no-load speed in Francis turbines

Hossein Hosseinimanesh[1], Christophe Devals[2], Bernd Nennemann[3] and François Guibault[2]

[1]Department of Mechanical Engineering, École Polytechnique de Montréal
CP 6079, succ. Centre-ville, Montréal, QC, H3C 3A7, Canada, hossein.hosseinimanesh@polymtl.ca
[2]Department of Computer Engineering, École Polytechnique de Montréal
CP 6079, succ. Centre-ville, Montréal, QC, H3C 3A7, Canada, christophe.devals@polymtl.ca, francois.guibault@polymtl.ca
[3]Andritz Hydro Canada Inc.
6100 Transcanadienne, Pointe-Claire, QC, H9R 1B9, Canada, bernd.nennemann@andritz.com

Abstract

No-load speed is an important performance factor for the safe operation of hydropower systems. In turbine design, the manufacturers must conduct several model tests to calculate the accurate value of no-load speed for the complete range of operating conditions, which are expensive and time-consuming. The present study presents steady and unsteady methods for calculating no-load speed of a Francis turbine. The steady simulations are implemented using a commercial flow solver and an iterative algorithm that relies on a smooth relation between turbine torque and speed factor. The unsteady method uses unsteady RANS simulations that have been integrated with a user subroutine to compute and return the value of runner speed, time step and friction torque. The main goal of this research is to evaluate and compare the two methods by calculating turbine dynamic parameters for three test cases consisting of high and medium head Francis turbines. Overall, the numerical results agreed well with experimental data. The unsteady method provided more accurate results in the opening angle range from 20 to 26 degrees. Nevertheless, the steady results showed more consistency than unsteady results for the three different test cases at different operating conditions.

Keywords: No-load speed, runaway speed, Francis turbine, steady-state simulation, unsteady state simulation.

1. Introduction

Hydropower manufacturers must guarantee the performance of the turbine runner at the end of the design process. Hence tests are performed on homologous models to demonstrate the guaranteed values of dynamic parameters such as the efficiency, cavitation, stability, runaway, and hydraulic axial thrust for the complete range of operating conditions. Among these parameters, runaway speed and no-load speed have an essential role in ensuring the safety of a power plant.

No-load speed is the maximum speed attained during no-load operation of a turbine-generator at maximum head. It is also called runaway speed at full gate opening. No-load and runaway conditions happen when the control system fails to close rapidly the vanes during a load rejection event, and this failure may lead to dangerous situations. The runner speed rises while there is no generator-load to dissipate the runner kinetic energy. Under such circumstances, slim structures such as turbine blades may be deformed due to increased centrifugal and hydraulic forces. Consequently, the rotor may become unbalanced and produce vibration, which can lead to failure of the entire turbine. Although the runaway and no-load conditions occur far from the turbine design operating condition, they constitute plausible events during an emergency situation such as a fault of the control system during emergency shutdown. Thus the accurate prediction of runaway speed and no-load speed at different wicket gate angles is necessary to ensure the structural integrity of turbine components and the safety of the hydropower plant.

Received January 15 2015; revised March 20 2015; accepted for publication July 18 2015: Review conducted by Prof. Soon-Wook Kim. (Paper number O15039S)
Corresponding author: Hossein Hosseinimanesh , hosseinimanesh747@gmail.com

This paper was presented at the 27th IAHR Symposium on Hydraulic Machinery and Systems, September 4, Montreal, Canada.

An accurate value of no-load speed is usually obtained from model tests, which are performed by the turbine manufacturers. Experimental tests are expensive and time-consuming. Thus it is desirable to develop alternative numerical methods for computing no-load speed of prototype turbines. For this purpose, hydro acoustic models are fast and robust, and allow simulating the dynamic behaviour of the complete hydropower plant. Nicolet [1] used a 1D hydro acoustic method for modelling the hydraulic components of a hydropower plant in both transient and steady modes. The model could show the evolution of turbine dynamic parameters such as angular speed, pressure and discharge during a load rejection event. However, this method depends on experimental data. For instance it requires the turbine hill-chart to determine hydraulic resistance and inductance needed in transient simulations.

Over the past two decades, industrial computational fluid dynamics (CFD) has been applied for solving difficult engineering problems because of computational capacity increase and numerical techniques advancements. Vu [2] used steady-state stage computations for accurate prediction of efficiency characteristics of a Francis turbine near its best efficiency point. He also showed steady-state simulations to be a highly effective methodology for comparing global draft tube performance for nearby design operating points [3]. Melot [4] performed steady-state stage simulations with RANS solver in order to compute the static stresses at speed no-load conditions. The computational domain included the casing, stay vane and runner passage and draft tube. The results were in good agreement with on-site strain gauge measurements. He concluded that the steady-state methodology is robust and flexible enough to be used in different projects under no-load condition during the design phase. Hosseinimanesh [5] used a methodology based on the steady-state RANS flow simulations in order to calculate no-load speed. The results showed good agreement with experiments.

In hydro turbines, unsteady CFD simulations have been used for analyzing highly turbulent flows at off-design conditions and transient processes. The results showed the existence of unsteady flow phenomena such as vortex break down, rotor-stator interaction and vortex shedding inside flow passage [6-9]. Kolšek [10] used unsteady flow simulations with the standard k-ε turbulence model to predict the angular speed, axial force and pressure at selected points during the shut-down of an axial water turbine. Nicolle [11] obtained the loading on the blades in a 3D transient numerical simulation of a hydraulic turbine during the start-up phase. The unsteady simulations included wicket gate motion and angular speed variation algorithms. Cherny [12] studied the transient behavior of Francis turbine during runaway using the unsteady stage simulations. He developed an approach, consisting of a one-dimensional water hammer calculation for the penstock and 3D unsteady periodic stage simulation for the turbine. The results showed that a periodic stage approach ignored the effects of the runner-stator interaction and damped the vortex rope in the draft tube. Li [13] simulated the no-load condition at 9 wicket gate angles for a Francis turbine with the RNG k-ε turbulence model. However, very little details were given about the results and numerical methods used. He reported the presence of intense swirling flow at the draft tube inlet, and secondary and transverse flows in the runner.

The present paper, which is an extension to the study presented at the 27th IAHR Symposium on Hydraulic Machinery and Systems [5], applies steady and unsteady RANS methodologies to accurately estimate turbine no-load speed and runaway in Francis turbines. The unsteady and steady methods are compared on three test cases over a range of operating conditions in order to introduce a robust methodology. The numerical results are validated using data obtained during model test measurements carried out by Andritz Hydro.

2. Computational aspect

2.1 Geometry and mesh description

The numerical study is performed on three test cases that include medium and high head Francis turbines in order to evaluate the capability of the proposed methodology. The high head Francis turbine comprises 20 stay vanes and guide vanes, 15 runner blades and draft tube. The medium head Francis turbine consists of 20 stay vanes and guide vanes, 13 runner blades and draft tube. The computational domain for all test cases encompasses a distributor channel (one stay vane, one wicket gate), a runner passage (hub, shroud, blade) and the draft tube as can be seen in Fig. 1 for test case 1. The summary of turbine characteristics is shown in Table 1. Test cases 2 and 3 consist of the same geometries for all components except the runner blade.

Table 1 Test case specifications.

	Runner type	Blades	Wicket gates	Stay vanes
Case 1	Medium head Francis turbine	1/13	1/20	1/20
Case 2	High head Francis turbine	1/15	1/20	1/20
Case 3	High head Francis turbine	1/15	1/20	1/20

The geometries and meshes of the components were generated using Andritz design tools. Multi-bloc-structured meshes for runner channel and draft tube, and hybrid meshes in a single channel for the wicket gate and stay vane were used. For example, Fig. 1 shows the computational mesh for each component for test case 1. The complete computational domain of test cases 1, 2 and 3 comprised 554k, 811k, and 813k mesh nodes respectively, as detailed in Table 2.

Table 2 Number of nodes for simulation domains.

	Stay vane & wicket gate	Runner blade	Draft tube	
Mesh type	Hexahedra and prisms	Hexahedra	Hexahedra	Total
Case 1	167k	144k	243k	554k
Case 2	170k	435k	206k	811k
Case 3	170k	437k	206k	813k

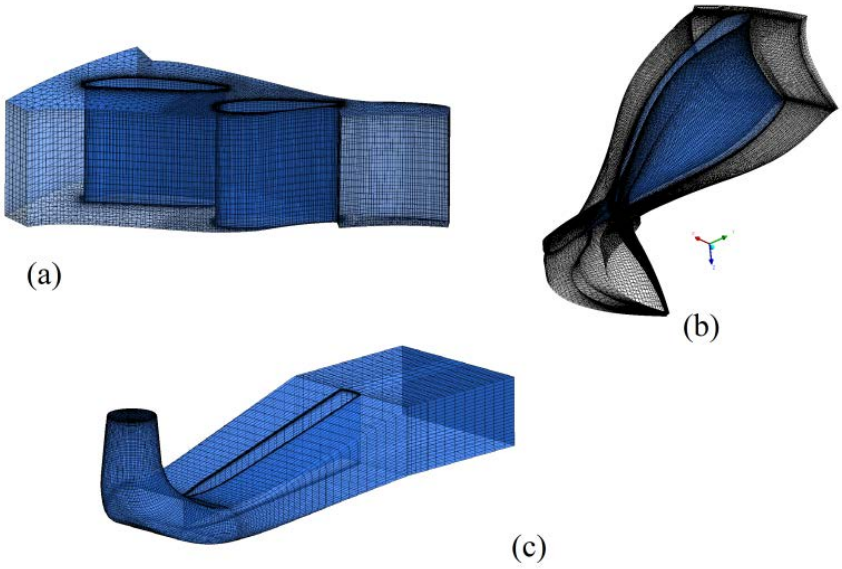

Fig. 1 Mesh for components (test case 1).

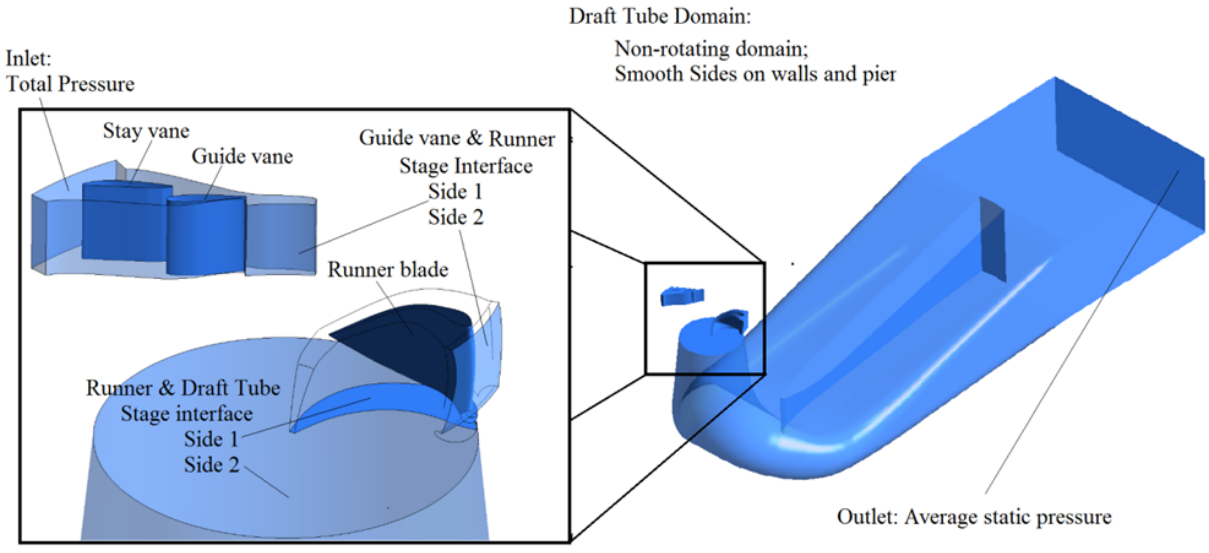

Fig. 2 Geometry and boundary conditions of computational domains (test case 1).

2.2 Numerical set-up

In the present study, the runaway speed is calculated by performing steady and unsteady Reynolds averaged Navier-Stokes 3D calculations at different operating conditions using Ansys-CFX 14 commercial solver. The Reynolds-averaged Navier-Stokes equations (RANS) are given by

$$\frac{\partial U_i}{\partial x_i} = 0 \tag{1}$$

$$\rho \frac{\partial U_i}{\partial t} + \rho \frac{\partial (U_j U_i)}{\partial x_j} = -\frac{\partial P}{\partial x_i} + f + \mu \left(\frac{\partial^2 U_i}{\partial x_j^2} \right) + \rho \frac{\partial}{\partial x_j} \overline{u_i' u_j'} \tag{2}$$

where U is the average velocity (m/s), ρ is the fluid density (kg/m^3), f is the body force per unit mass of fluid (N), μ is the dynamic viscosity of water (N s/m^2), P is the average pressure (N/m^2), and $\rho \overline{u_i' u_j'}$ is the Reynolds shear stress (N/m^2), which can be written based on the Boussinesq hypothesis [14] as:

$$\rho \overline{u_i' u_j'} = -\mu_t \left(\frac{\partial u_i}{\partial x_j} + \frac{\partial u_j}{\partial x_i} \right) + \frac{2}{3} \rho \delta_{ij} k \tag{3}$$

where $k = \frac{1}{2} \sqrt{\overline{u_i' u_i'}}$ is the turbulent kinetic energy, and δ_{ij} is the Kronecker delta, μ_t is the turbulent viscosity.

The standard k-ε turbulence model is applied for treating turbulence. The standard k-ε model is known as a reliable and robust turbulence model for simulating high Reynolds number flows in Francis turbines. Galvan's [15] investigation on the steady state swirling flow in a draft tube showed that the standard k-ε turbulence model demonstrates good balance between reliable performance and computational cost.

The standard k-ε model is based on two transport equations, one for turbulent kinetic energy k, and the other for the turbulent dissipation ε. The transport equations for turbulent kinetic energy, k, and its dissipation rate, ε, are written as:

$$\frac{\partial \rho k}{\partial t} + \frac{\partial (\rho U_j k)}{\partial x_j} = \frac{\partial}{\partial x_j} \left[\left(\mu + \frac{\mu_t}{\sigma_k} \right) \frac{\partial k}{\partial x_j} \right] + P_k - \rho \varepsilon \tag{4}$$

$$P_k = \rho \overline{u_i' u_j'} \frac{\partial \rho U_i}{\partial x_j} \tag{5}$$

$$\frac{\partial \rho \varepsilon}{\partial t} + \frac{\partial (\rho U_j \varepsilon)}{\partial x_j} = \frac{\partial}{\partial x_j} \left[\left(\mu + \frac{\mu_t}{\sigma_\varepsilon} \right) \frac{\partial \varepsilon}{\partial x_j} \right] + C_{\varepsilon 1} P_k \frac{\varepsilon}{K} - \rho C_{\varepsilon 2} \frac{\varepsilon^2}{K}. \tag{6}$$

The standard k-ε model equations include the empirical constants σ_k=*1.0*, σ_ε=*1.3*,$C_{\varepsilon 1} = 1.44$, and $C_{\varepsilon 2}$=*1.92*.
The turbulent viscosity is expressed by:

$$\mu_t = \rho C_\mu \frac{k^2}{\varepsilon} \tag{7}$$

where C_μ =0.09 is a constant number.

The momentum and turbulent advection equations have been discretized using the high-resolution scheme and first-order scheme, respectively. The steady stage simulations were performed using one distributor channel as a stationary component and a runner blade passage as a rotating component in order to improve the computation cost. A stage interface was used for connecting the runner and distributor channel, and also the runner and draft tube modeled in distinct frames of reference. Radial runner blade passage interfaces were connected through fully matching rotational periodicity model. The scalable wall function was used, and mesh densities were chosen such that the mean value of y^+ remains in the range recommended by the flow solver. The inlet boundary condition was set to the total pressure associated to the turbine net head. The outlet boundary condition was specified as zero-averaged static pressure. No-slip boundary condition was imposed for all solid walls.

2.3 Methodologies

2.3.1 Steady state method

The steady state methodology is based on the hypothesis that the turbine torque is a smooth function of the speed factor. In order to find runaway and no-load speed, we have to find the zero of the function. A general pseudo-code of the proposed methodology is shown in algorithm 1. The first step consists in generating meshes from parametric geometry descriptions of each component. Then the numerical set-up is implemented as described in the previous section for the selected wicket gate angle. In step 3, we initialize the simulations for two operating point speed factors, $N_{ed,1}$ and $N_{ed,2}$ with best efficiency point speed value and 1.3 times of the same value, respectively. Then steady stage computations are performed for those points. In step 5 the blade torques T_1, T_2, and power factor $P_{ed,2}$ are derived from the converged simulations. Then we initialize the loop control value to 2 and start to compute the no-load speed in an iterative way as follows.

At the beginning, when $n = 2$, there are only two known points, namely $(N_{ed,1}, T_1)$ and $(N_{ed,2}, T_2)$. If the two points have the same sign for the torque, we use the secant method that passes a line through two points, and takes where it intersects abscissa as next point. Otherwise, we use the false position method. If $n > 2$, there are many known points $(N_{ed,1}, T_1), \ldots, (N_{ed,n}, T_n)$, which lead to more available methods to estimate $N_{ed,n+1}$ such that T_{n+1} would be equal to zero. The simplest method is to use the last two points $(N_{ed,n}, T_{n-1})$ and $(N_{ed,n}, T_n)$, and to compute $N_{ed,n+1}$ using again the secant method until two points of unlike torque sign are obtained. Afterward, the best choice is to use the false position method. This approach is proved to be efficient for calculating runaway speed.

In order to do fewer iterations of the main loop in algorithm 1, and to do fewer numerical simulations with Ansys CFX, some attempts were done to use more than the last two points, for example, by using a linear regression through the last three or four points

or quadratic fitting of the last three points. These more complex approaches have not shown any significant advantage over the simple 2 point method.

The process is considered to have converged, and $N_{ed,n}$ is considered as the no-load speed if one of the following conditions is satisfied.

- $\frac{|N_{ed,n} - N_{ed,n-1}|}{N_{ed,n-1}} < 2\ \%$ for the two last points with different torque sign.
- The value of power factor $|P^*_{ed,n}|$ is less than 0.01.

Otherwise, we iterate, and compute the next operating condition, or stop if the loop control value n reaches the maximum value. Moreover, at each steady state simulation, the convergence tolerances of all main primitive variables were set to 10E-5 on the root mean square (RMS) residuals. Besides, the quantities of torque and inflow were tracked during simulation at monitoring points. Whenever their averaged values became steady, the simulation was considered to have converged.

Algorithm 1 Steady state methodology algorithm for no-load speed computing

Input: Wicket gate angle
Output: Runaway speed
1: Generate meshes
2: Numerical set-up
3: Initialize: Select speeds of two operating conditions $N_{ed,1}$, $N_{ed,2}$
4: Perform steady simulation for these two selected operating conditions
5: Compute torques T_1 , T_2, power factor $P_{ed,2}$ from steady simulation results
6: Set $n = 2$
7: **While** Simulation not converged **do** Steps 7.1-7.4
    7.1: From previous points $(N_{ed,n}, T_n)$, $(N_{ed,n-1}, T_{n-1}), \dots,$ compute the next operating condition at $N_{ed,n+1}$
    7.2: Perform steady simulation at $N_{ed,n+1}$
    7.3: Derive torque $T_{n+1}$and power coefficient $P_{ed,n+1}$
    7.4: Set $n = n + 1$
8: $N_{ed,\ no-load} = N_{ed,n}$

2.3.2 Unsteady method

In this method, an unsteady simulation is carried out at specific operating points until the turbine reaches the no-load condition. For unsteady simulation, the operating points are calculated using the angular momentum equation for the rotating mass as follows:

$$T - T_g = I_z \frac{d\omega}{dt} \tag{8}$$

Here T denotes the torque of turbine hydraulic force (Nm), T_g is the torque of the electromagnet or payload torque (Nm), I_z is the moment of inertia of the runner (kgm^2), and ω is the runner angular speed (rad/s). When a load rejection event occurs within a hydropower plant, the electromagnetic torque instantaneously drops to zero ($T_g = 0$), and the angular speed of the runner starts to rise monotonically. However, the rate of increase in angular speed eventually decreases because of hydraulic losses in the hydraulic system. Finally, the turbine angular speed reaches a maximum value, called the no-load speed. Under such circumstances, the runner moment tends to zero because of the balance between hydraulic and drag forces acting on the turbine.

Algorithm 2 presents the unsteady methodology for estimating the runaway and no-load speed in Francis turbines. The steps from 1 to 4 are similar to the steady state methodology. We similarly generate meshes and implement the numerical set-up, but perform the steady stage simulation only at the speed factor of the best efficiency point $N_{ed,1}$. In step 5 the blade torque T_1 is derived from the converged simulations. Then we initialize the loop control value to 2 and start to perform an unsteady stage simulation during which the operating points $N_{ed,n}$, are updated by

$$\omega_n = \omega_{n-1} + \frac{T_n \Delta t}{I_z} \tag{9}.$$

Equation (9) is derived from eq. (8) by a first order explicit discretization. In eq. (9), Δt represents a time step (s) that is adjusted automatically by eq. (10) based on the runner angular speed variation during no-load simulations:

$$\Delta t = \frac{M}{\omega \cdot a} \tag{10}$$

where ω (rad/s) is the runner angular speed, a=57.2958 deg/rad is a constant number. Furthermore, M =4° is a constant number corresponding to the angular variation in degrees at each time step.

All processes in Algorithm 2 are implemented using the commercial flow solver Ansys CFX. In simulations, the flow solver integrates a user subroutine written in Fortran 77 in order to compute and return the value of angular velocity, time step and friction torque.
For the unsteady computation to be considered converged at the no-load condition, the following conditions must be satisfied:

- $\frac{|N_{ed,n} - N_{ed,n-1}|}{N_{ed,n-1}} < 2\ \%$
- $\left|\frac{P_{ed,n}}{P_{ed,BEP}}\right| < 1\ \%$

Otherwise, we continue unsteady simulation for the next operating condition, or stop if the loop control value n reaches the maximum value.

Algorithm 2 Unsteady state methodology algorithm for no-load speed computing

Input: Wicket gate angle
Output: Runaway speed, inlet flow rate, pressure magnitude on the blade
1: Generate meshes
2: Numerical set-up
3: Select speed of an operating conditions $N_{ed,1}$
4: Perform steady simulation for the selected operating condition
5: Compute torque T_1, from steady simulation results
6: Set $n = 2$
7: **While** Simulation not converged **do** Steps 7.1-7.4
  7.1: From previous point $(N_{ed,n-1}, T_{n-1})$ compute the next operating condition at $N_{ed,n}$
  7.2: Continue unsteady simulation at $N_{ed,n}$
  7.3: Compute torque T_n and power factor $P_{ed,n}$
  7.4: Set $n = n + 1$
8: $N_{ed,\ no-load} = N_{ed,n}$

2.3.3 Friction torque

In eq. (8), the torque is calculated by

$$T = T_t(t) - T_{fr}(t) \tag{11}$$

where T_t, which is the turbine torque caused by pressure and viscous forces on the runner blade, is obtained from steady simulation results. The T_{fr} term, which is the friction torque on the turbine crown and band, is opposing the driving torque during no-load condition. The friction torque is calculated as follows:

$$T_{fr} = T_{fr,crown} + T_{fr,band}. \tag{12}$$

The friction torques $T_{fr,crown}$ and $T_{fr,band}$ have an impact on the crown and band sections, respectively. The friction torque impact on the crown surface is estimated using a model that was established based on the approximation of a smooth rotating disk in a housing with turbulent flow[16]. The friction torque on the crown is estimated by

$$T_{fr,crown} = \frac{C_m \rho \omega^2 r_{crown}^5}{2} \tag{13}$$

where ω is the runner angular velocity (rad/s), r_{crown} is the runner leading edge radius at the crown, ρ is the water density (kg/m^3), and C_m is the torque coefficient, defined as

$$C_m = 0.0311 \left(\frac{1}{Re^{0.2}}\right)\left(\frac{r_{crown}}{GAP_C}\right)^{0.1} \tag{14}$$

where GAP_C is the width of the runner crown clearance (m), and Re is the Reynolds number, which is equal to

$$Re = \frac{\omega \rho r_{crown}^2}{\mu} \tag{15}$$

In order to calculate the band torque, the band rotation was approximated by two concentric cylinders with the inner cylinder rotating with angular velocity ω, and the outer cylinder at rest. In the present work, Bilge's equation [17], which is an empirical relation of torque coefficient of coaxial cylinders, was applied for calculating the runner torque as follow:

$$T_{fr,band} = \frac{C_n \rho \pi \omega^2 \bar{r}_{band}^4 \cdot l_i}{2} \quad (16)$$

where l_i is the band seal length, and $\bar{r}_{band}$ is the average band radius. The moment coefficient for turbulent flow regimes with $Re > 10^4$ is defined as

$$C_n = 0.065\left(\frac{Gap}{\bar{r}_{band}}\right)^{0.3}(Re)^{-0.2} \quad (17)$$

where $Re = \frac{\rho \omega Gap \bar{r}_{band}}{\mu}$ is the Couette Reynolds number, Gap is the width of the runner band clearance, and $\bar{r}_{band}$ is the average radius of the band.

3. Results

3.1 Engineering parameters

The steady and unsteady approaches were applied on three test cases in order to assess the accuracy of the proposed methodologies. For each test case, we numerically calculated the dynamic parameters such as the speed factor N_{ed}, discharge factors $Q_{ed,}$ and power factor P_{ed}, defined by [18], at no-load condition for different opening angles. The numerical results were compared with experimental measurements.

Figure 3. (left) compares the experimental and numerical speed factors at no-load condition for different wicket gate angles. The unsteady approach led to more accurate estimates of the speed factor at wicket gate angles between 20 and 26 degrees. For instance, in case 2, the maximum discrepancies between CFD results and experiments were 3.42% and 3.95% in the unsteady and steady methods, respectively at the wicket angle of 26 degrees. Nevertheless, it is observed in Fig. 3 that the steady method resulted in more accurate predictions at wicket gate angle of 15 degrees compared to unsteady. The maximum differences between numerical and experimental speed factors for all cases are shown in Table 3.

Furthermore, Fig. 3 (right) shows the numerical and experimental results of the discharge factors at no-load condition. In Fig. 3, for case 1, the steady and unsteady results agreed well with experimental data. In a similar manner to the speed factor results, the unsteady method generates more accurate discharge factors in the opening angle range from 20 to 26 degrees for cases 2 and 3. For example, in case 2, the maximum discrepancies were 4.8% and 6% in the unsteady and steady methods for wicket angle of 26 degrees, respectively.

Figure 4. compares the no-load speed lines, which were computed from steady, unsteady and experimental methods. For all test cases, the no-load speed lines follow the same trend, but a little deviation is observed for higher speed factors. For case 1, the steady and unsteady lines are very close to each other. For case 2 and 3, the steady lines are closer to experiments.

The unsteady method was not as accurate as the steady method in its prediction for wicket gate angles below 20 degrees. In order to explain the prediction error for those angles, the flow physics, computed by the steady and unsteady simulations for one such operating condition, are analyzed and compared.

Figure 5. shows the distribution of normalized axial velocity, surface streamlines and velocity vectors in a plane section of the draft tube, computed through steady and unsteady simulations, at a wicket gate opening of 15 degrees for case 2. The same overall flow behavior is observed in the draft tube for both methods. In Fig. 5, the turbine discharge enters near the draft tube cone wall. On the other hand, a mainly axial flow returns towards the runner in the cone center. Furthermore there is a flow moving towards the draft tube outlet. Comparison between simulations shows that the unsteady simulation calculated a backflow region with a higher velocity near the draft tube cone and an entering flow with a lower velocity near the cone wall compared to the steady simulation.

Figures 6. and 7 present the surface streamlines and the normalized velocity contours, computed using steady and unsteady simulations, at 1 % and 50 % runner blade span, respectively for the same operating point. Fig. 6 (left) shows that a high velocity flow passes the turbine passage at 1 % span in the steady simulation. On the other hand, the right part of Fig. 6 shows that low velocity vortices have blocked a part of the turbine passage in the unsteady simulation. In Fig. 7 both simulations calculated the same flow pattern at 50 % span. Fig. 7 shows that strong axial vortices have blocked the largest part of the inlet runner passage.

Overall, it can be noted that the unsteady simulation has over predicted the turbine blockage at 1 % span for a wicket gate opening angle of 15 degrees. This over prediction caused lower turbine discharge, and no-load speed compared to experimental and steady results. This over prediction may be caused by the presence of the stage averaging interface between the runner and draft-tube. It is expected to obtain more accurate results by performing unsteady simulations in a fluid domain with a very fine meshes and smaller time steps and using a transient rotor-stator interface.

Generally, from the results, it appears that the no-load speed was well predicted through the proposed methodologies. Nevertheless, the engineering parameters, calculated by the steady method display more consistency than the unsteady results for the three different test cases at different operating conditions. Hence the steady method can be used as a reliable and precise tool for computing runaway and no-load speed in Francis turbines.

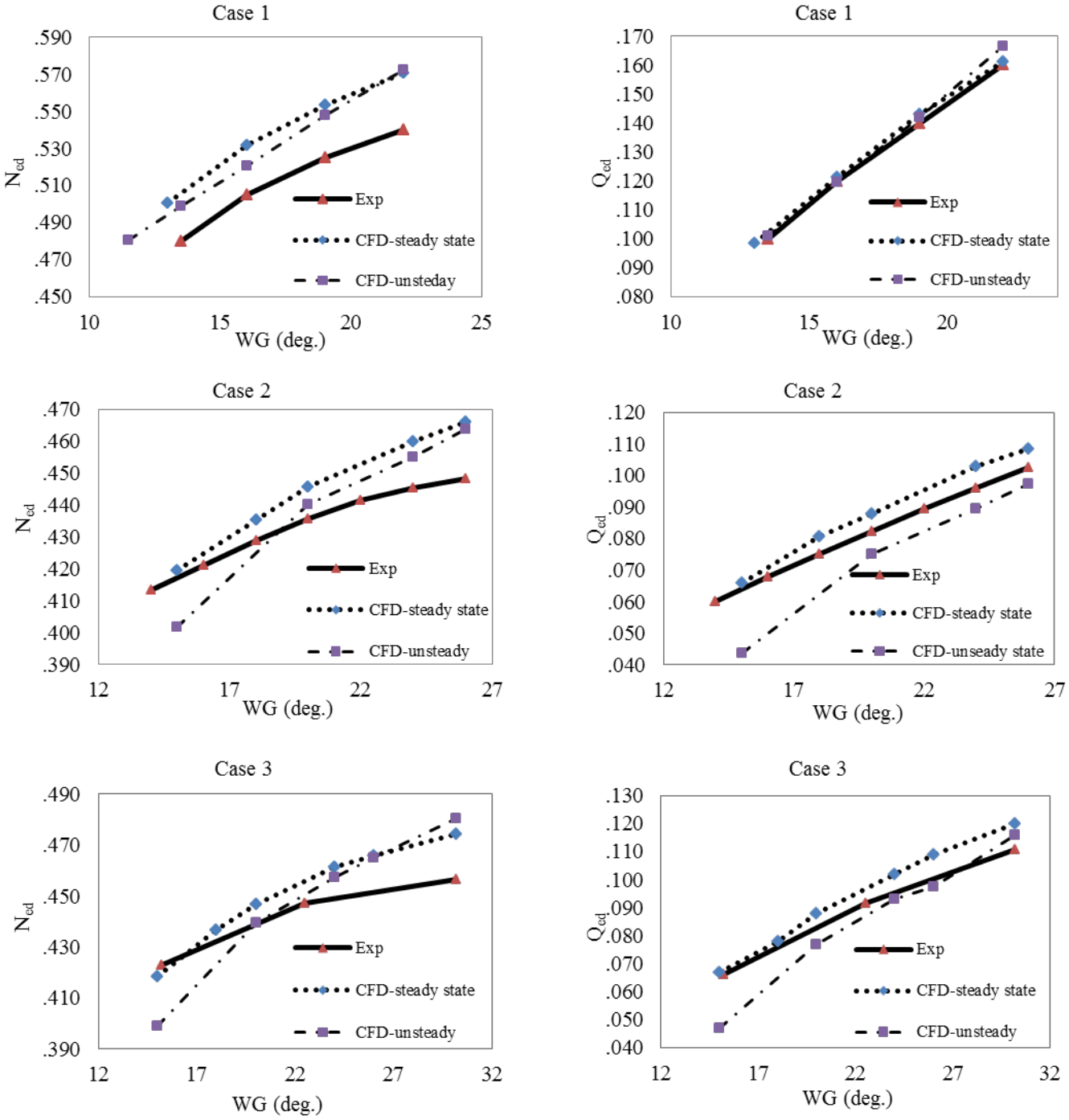

Fig. 3 Speed factor N_{ed} & discharge factor Q_{ed} vs. wicket gate angles (WG) from CFD and experiments at no-load speed

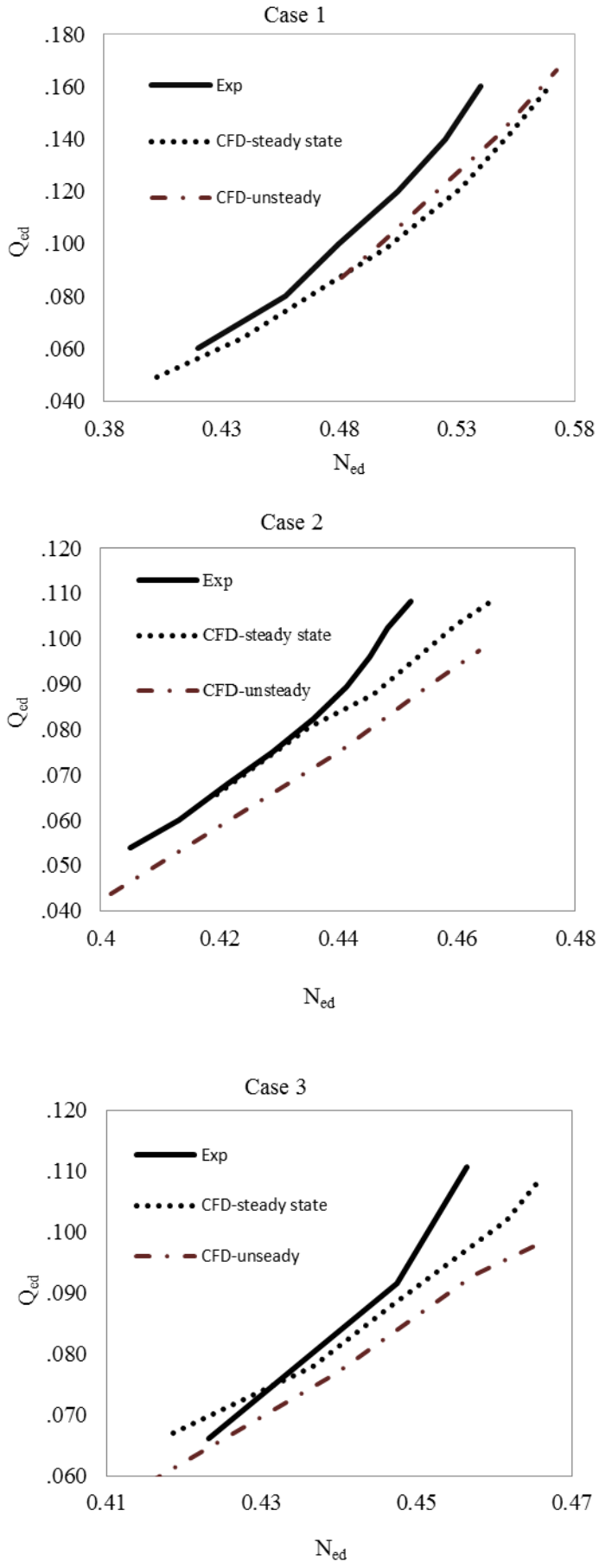

Fig. 4 No-load speed line computed from CFD and experiments

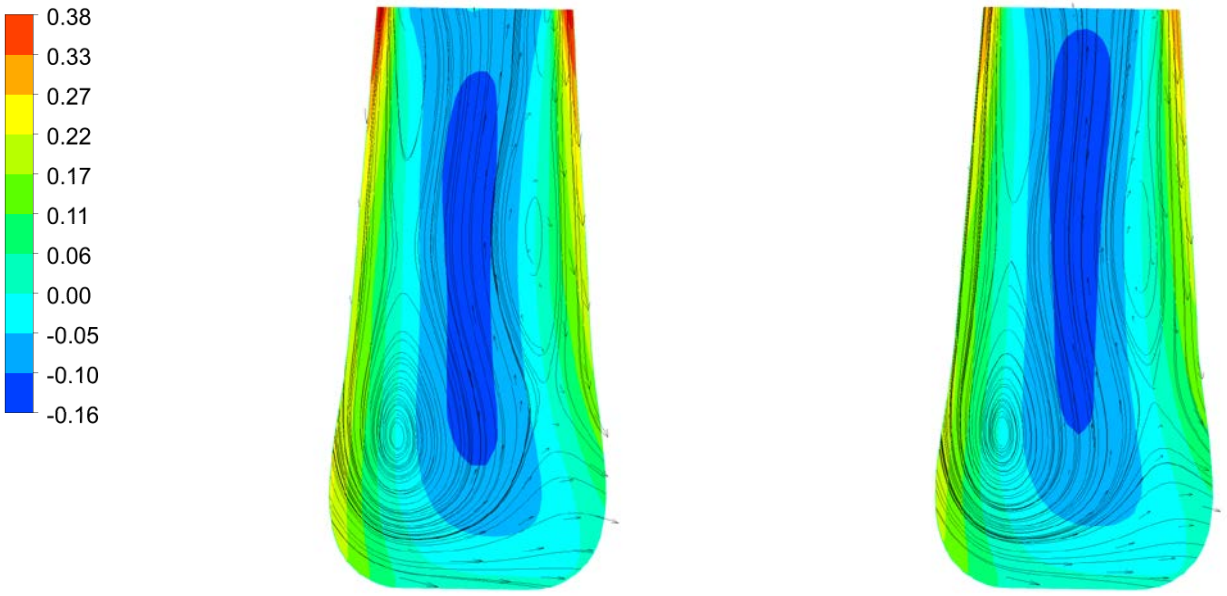

Fig. 5 Normalized axial velocity field, velocity vectors and streamlines on a section plane crossing the draft tube in steady (left) and unsteady (right) simulations at wicket gate angle of 15 degrees case 2

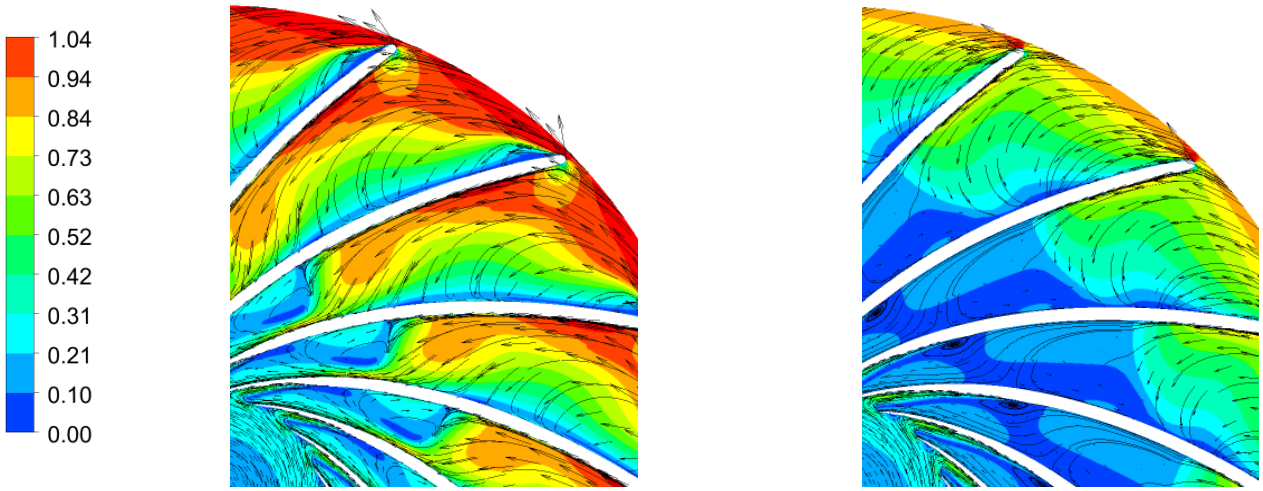

Fig. 6 Comparison normalized velocity field and 2D streamlines between steady (left) and unsteady (right) simulations at wicket gate angle of 15 degrees at 1% span case 2

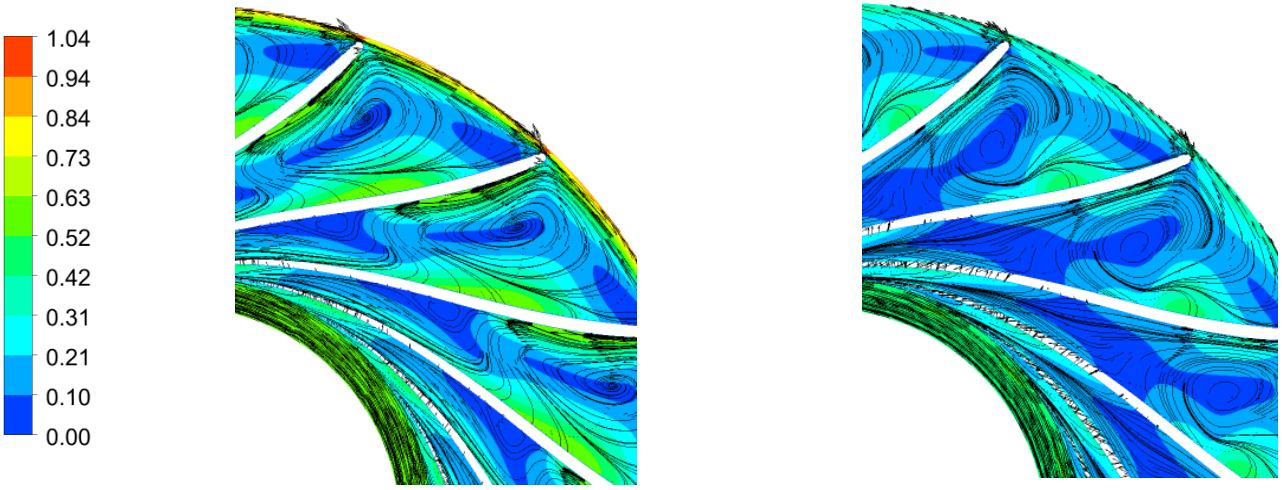

Fig. 7 Comparison normalized velocity field and 2D streamlines between steady (left) and unsteady (right) simulations at wicket gate angle of 15 degrees at 50% span case 2

Table 3 Maximum discrepancy between the numerical and experimental speed factors.

Case	Wicket gate opening	Discrepancy	
		Steady state	Unsteady state
1	22°	5.65 %	5.99%
2	26°	3.95 %	3.42 %
3	26°	3.23 %	2.87 %

3.2 Accuracy and convergence analysis of the steady-state algorithm

In order to analyze the accuracy and convergence properties of the two proposed algorithms, the convergence behavior of the steady-state algorithm is further discussed. According to the proposed methodology, steady-state computations are performed at operating points that are selected based on the false position method. The computations are stopped when the turbine torque and efficiency become small enough. Fig. 8 shows the evolution of the power factor P_{ed}, which corresponds to turbine torque and angular speed, for selected operating points. In Fig. 8 (left), the power factor decreases gradually when the speed factor increases in runaway speed computations. The points close to the Ned-axis are shown in Fig. 8. (right). They show that when approaching runaway speed, a large drop of the power factor occurs for a small increase of the speed factor. For instance, the power factor decreases by 335% between E_1 and E_2, while the speed factor simultaneously increases only by 0.09%, as detailed in Table 4.

The sudden drop of the power factor near the horizontal axis illustrates the highly non-linear behavior of the flow near the no-load condition. This sharp deviation in the power factor reduces the capacity of the steady-state algorithm to precisely determine the speed coefficient at which torque becomes zero. This observation justifies the choice made in the present study, whereby results for the power factor are bounded within a range from -0.01 to 0.01 around zero, which was determined suitable for predicting the runaway speed with an adequate level of accuracy.

Table 4 Maximum variation of dimensionless parameters near the N_{ed}-axis.

Wicket gate opening	Points	N_{ed}	P_{ed}
15°	E_1-E_2	0.09 %	-335 %
18°	F_1-F_2	0.16 %	-193 %

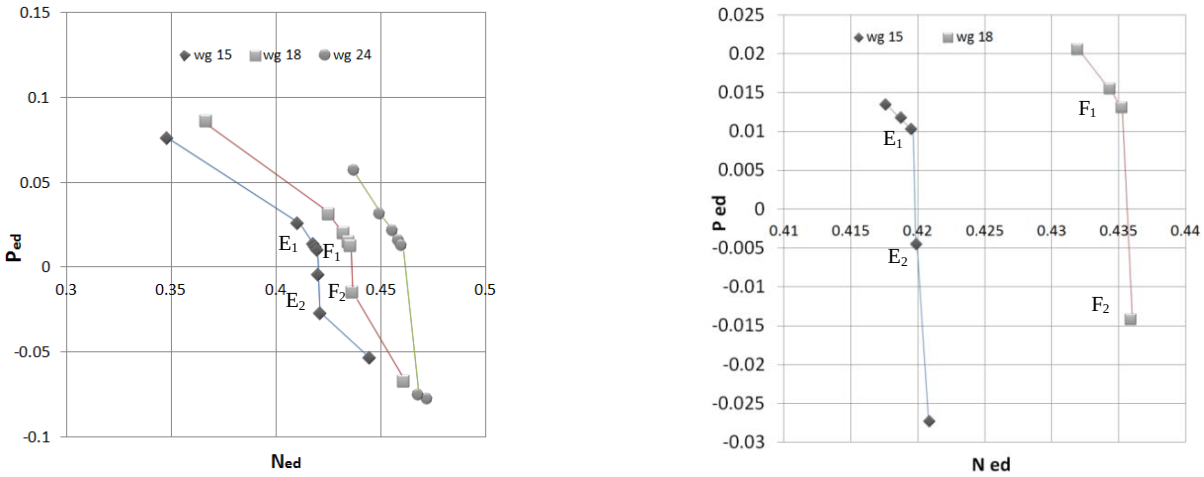

Fig. 8 Power factor P_{ed} vs. speed factor Ned for test case 2 in steady simulations.

3.3 Convergence of the unsteady simulation algorithm

Contrary to the steady-state case, the algorithm used in the unsteady methodology does not require to accurately determine the condition for which torque becomes zero. The algorithm must, however, detect a stabilization of the speed factor. The flow behavior being highly unsteady, the level at which stabilization occurs may vary depending on the starting point of the simulation. To test the sensitivity of the unsteady solution to its starting point, two different simulations were performed with the different starting points on the second case at the opening angle of 15 degrees. The main goal was to evaluate the repeatability of the unsteady methodology. First unsteady simulation started from a converged steady method solution, while the second unsteady simulation began from the best efficiency operating point.

Figure 9. shows the evolution of the speed factor during the first simulation. In Fig. 9, the no-load speed was primarily calculated by steady method that started from point A (N_{ed} *=0.35*), and converged to point B (N_{ed}*=0.41*) through five steps. Afterward, an unsteady simulation started from point B, which finally converged to point C (N_{ed} *= 0.398*). The difference of 4.8 percent was found between speed factors calculated by steady and unsteady methods in Fig. 9.

Figure 10. shows the evolution of speed factors during the second simulation. At the first step, a steady state simulation was performed at point D, the best efficiency operating point, in order to obtain an initial solution. After convergence of the steady simulation, the unsteady simulation is started from E with speed factor of best efficiency operating point. In Fig. 10, the speed

factor increased at the beginning of unsteady simulation due to load rejection. Eventually, it decreased and converged to point F (*Ned=0.399*). The discrepancy between speed factors in the first and second unsteady simulations was 0.25 %. This little discrepancy between unsteady simulations with different starting points shows that the applied unsteady methodology is fairly successful in reproducing the results.

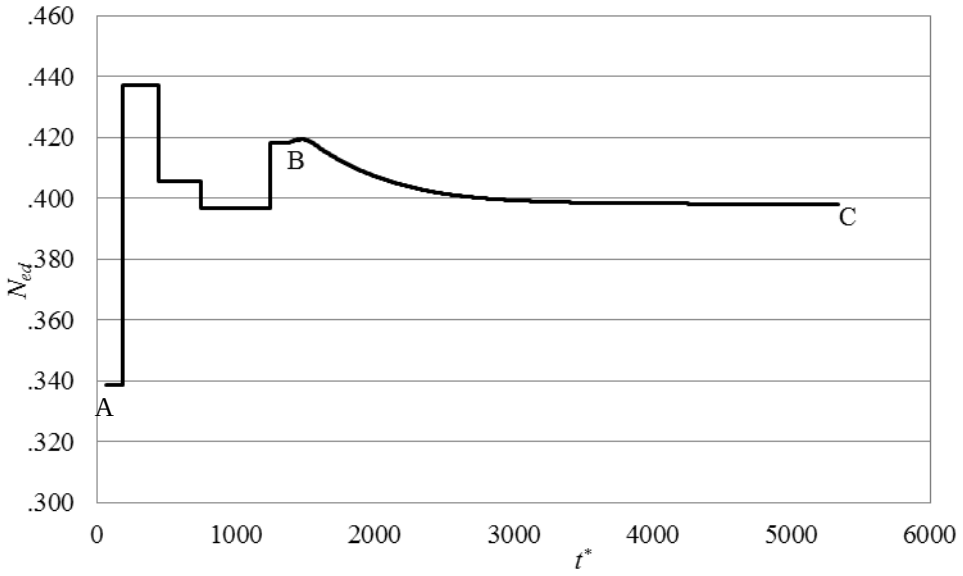

Fig. 9 Speed factor N_{ed} vs dimensionless accumulated time step t^* by steady and unsteady methods

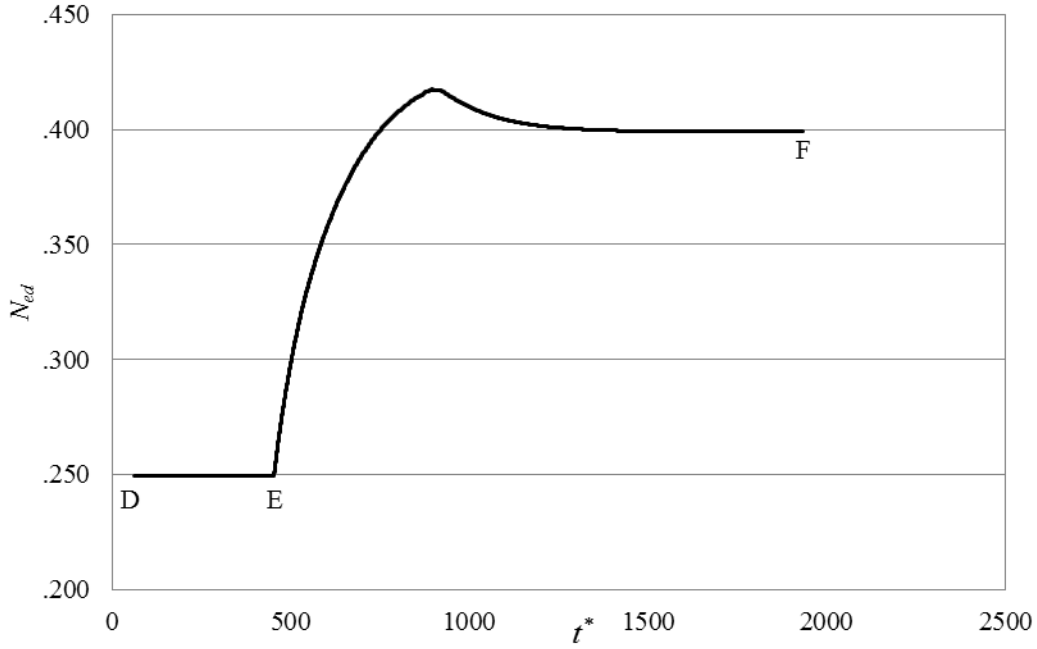

Fig. 10 Speed factor N_{ed} vs dimensionless accumulated time step t^* by unsteady method

4. Conclusion

In a runner design process, the accurate determination of runaway and no-load speed is important to ensure the safe operation of the hydropower plant. Hence this paper evaluated a steady and an unsteady method for computing the no-load speed of Francis turbine runners at different opening angles. The steady method was faster and simpler than the unsteady method because it used steady-state stage computations and a simple algorithm based on the smooth relation between torque and speed. The unsteady method relied on unsteady state computations in a CFD flow solver that integrated a user subroutine in order to retrieve the value of angular velocity during simulation. The unsteady simulations depended on significant computational effort to compute accurate

values of runaway speed due to difficulties related to unsteady turbulent flow modelling and instabilities.

Two methods were assessed by calculating turbine dynamic parameters: speed factor, discharge factor and power factor during runaway speed for three test cases consisting of high and medium head Francis turbines. Overall, the numerical results agreed well with experimental data. The unsteady method provided more accurate results in the opening angle range from 20 to 26 degrees for all cases. However, the unsteady method was not successful for wicket gate angles lying outside this range. For instance, the study of flow simulation results showed that the unsteady simulation over predicted the flow blockage in the turbine passage at a wicket gate opening angle of 15 degrees in case 2.

Furthermore, some parts of the error corresponded to the stage interface model, used for connecting the rotating and stationary parts in the steady and unsteady simulations. The stage interface model neglected some transient effects because of performing the circumferential averaging of the fluxes at the interface. A transient rotor-stator model, which simulates the relative motion between components on each side of the interfaces, may increase the no-load speed prediction accuracy.

Furthermore, in the present study very little discrepancy was found between unsteady simulations with different starting points for the same wicket gate angle in case 2. It showed the repeatability of the applied unsteady methodology in order to compute the no-load speed.

Generally, the steady results showed more consistency than unsteady results in the three different test cases at different operating conditions. In addition, there were difficulties related to the unsteady simulation convergence, which led to more expensive computational efforts compared to steady method. Hence the steady method can be applied by design engineers as a reliable tool in order to compute runaway speed in a wide range of operating conditions with an adequate level of accuracy.

Acknowledgments

The Authors are grateful to the ANDRITZ Hydro for technical support of the project, and would like to thank Dr. Julien Dompierre for providing his useful comments and valuable knowledge about the numerical analysis in this project.

Nomenclature

$C_{\varepsilon 1}$	Constant number(=*1.44*)
$C_{\varepsilon 2}$	Constant number(=*1.92*)
C_{μ}	Constant number(=*1.92*)
C_m	Torque coefficient= $0.0311\left(\frac{1}{Re_1^{0.2}}\right)\left(\frac{r_{crown}}{GAP_C}\right)^{0.1}$
C_n	Torque coefficient= $0.065(\frac{Gap}{\bar{r}_{band}})^{0.3}(Re)^{-0.2}$
D	Turbine throat diameter (m)
f	Body force of unit mass fluid (N)
$\mathrm{GAP_C}$	Runner crown clearance (m)
Gap	Width of the runner band clearance
H	Turbine net head (m)
I_z	Moment of inertia of the runner (kgm^2)
k	Turbulent kinetic energy(= $\frac{1}{2}\sqrt{\overline{u_i'u_i'}}$)
l_i	Band seal length
M	Constant number corresponding to the angular variation in degrees at each time step (=4)
n	Loop control value
N_{ed}	Speed factor, Energy Units
P	Average pressure (N/m^2)
$P^*_{ed,n}$	Dimension less Power factor, (= $\frac{P_{ed,n}}{P_{ed,BEP}}$)
P_{ed}	Power factor, Energy Units
Q_{ed}	Discharge Factor
$\bar{r}_{band}$	Average band radius
r_{crown}	Runner leading edge radius at the crown
Re	Reynolds number (=U_bD_h/ν)
Re_1	Reynolds number(= $\frac{\omega\rho r_{crown}^2}{\mu}$)
Re_2	Reynolds number(= $\frac{\rho\omega Gap\bar{r}_{band}}{\mu}$)
T	Turbine torque(Nm)
$T_{fr,crown}$	Friction torques on crown(= $\frac{C_m\rho\omega^2 r_{crown}^5}{2}$)
$T_{fr,band}$	Friction torque on band(= $\frac{C_n\rho\pi\omega^2\bar{r}_{band}^4 \cdot l_i}{2}$)
T_g	Torque of the electromagnet(Nm)
t^*	Dimensionless accumulated time step
U	Average velocity (m/s)
V_{ref}	Reference velocity, m/s (= $\sqrt{gH}$)
V^*	Normalized velocity *(= V/V_{ref})*
ρ	Fluid Density (kg/m^3)
$\rho\overline{u_i'u_j'}$	Reynolds shear stress (N/m^2)
f	Body force of unit mass fluid (N)
δ_{ij}	Kronecker delta
σ_k	Constant number (=1.0)
ω	Runner angular speed (rad/sec)
σ_ε	Constant number(=*1.3)*
μ_t	Turbulent viscosity
μ	Dynamic viscosity of water (N s/m^2)

References

[1] Nicolet, C., Arpe, J., and Avellan, F., 2004, "Identification and Modeling of Pressure Fluctuations of a Francis Turbine Scale Model at Part Load Operation," Proceedings of the 22nd IAHR Symposium on Hydraulic Machinery and Systems.

[2] Vu, T. C., and Retieb, S., 2002, "Accuracy assessment of current CFD tools to predict hydraulic turbine efficiency hill chart," Proceedings of the 21st IAHR Symposium on Hydraulic Machinery and Systems, pp. 193-198.

[3] Vu, T. C., Devals, C., Zhang, Y., Nennemann, B., Guibault, F., 2011, "Steady and unsteady flow computation in an elbow draft tube with experimental validation," International Journal of Fluid Machinery and Systems, 4(1), pp. 85-96.

[4] Melot, M., Monette, C., Coutu, A., and Nennemann, B., 2014, "A new standard Francis runner design procedure to predict static stresses stresses at speed-no-load," Hydropower Dams (1).

[5] Hosseinimanesh, H., Vu, T. C., Devals, C., Nennemann, B., and Guibault, F., 2014, "A steady-state simulation methodology for predicting runaway speed in Francis turbines," IOP Conference Series: Earth and Environmental Science, 16(3), 032044.

[6] Ruprecht, A., Helmrich, T., Aschenbrenner, T., and Scherer, T., 2002, "Simulation of vortex rope in a turbine draft tube," Proceedings of the 21st IAHR Symposium on Hydraulic Machinery and Systems.

[7] Guo, C., Wang, G., and Xiao, J., 2009, "Numerical Simulation for Hydraulic Characteristics of Cylindrical Valve in Runaway Protection Process," Proceedings of Power and Energy Engineering Conference, APPEEC. Asia-Pacific, pp. 1-4.

[8] Levchenya, A. M., Smirnov, E. M., and Goryachev, V. D., 2010, "RANS-based numerical simulation and visualization of the horseshoe vortex system in the leading edge endwall region of a symmetric body," International Journal of Heat and Fluid Flow, 31(6), pp. 1107-1112.

[9] Nennemann, B., Vu, T. C., and Farhat, M., 2005, "CFD prediction of unsteady wicket gate-runner interaction in Francis turbines: A new standard hydraulic design procedure," HYDRO 2005 International Conference and Exhibition Villach, Austria.

[10] Kolšek, T., Duhovnik, J., and Bergant, A., 2006, "Simulation of unsteady flow and runner rotation during shut-down of an axial water turbine," Journal of Hydraulic Research, 44(1), pp. 129-137.

[11] Nicolle, J., Morissette, J. F., and Giroux, A. M., 2012, "Transient CFD simulation of a Francis turbine startup," IOP Conference Series: Earth and Environmental Science, 15(6), 062014.

[12] Cherny, S., Chirkov, D., Bannikov, D., Lapin, V., Skorospelov, V., Eshkunova, I., and Avdushenko, A., 2010, "3D numerical simulation of transient processes in hydraulic turbines," IOP Conference Series: Earth and Environmental Science, 12(1), 012071.

[13] Li, J., Yu, J., and Wu, Y., 2010, "3D unsteady turbulent simulations of transients of the Francis turbine," IOP Conference Series: Earth and Environmental Science, 12(1), 012001.

[14] Davidson, P. A., 2004, Turbulence: an introduction for scientists and engineers, Oxford University Press.

[15] Galvan S , Reggio M , and Guibault F, 2011, "Assessment study of k-E turbulence models and near-wall modeling for steady state swirling flow analysis in a draft tube using Fluent," Engineering Applications of Computational Fluid Mechanics, 5, pp. 459-478.

[16] Schlichting, H., and Gersten, K., 2000, Boundary-Layer Theory, MacGraw-Hill.

[17] Bilgen, E., and Boulos, R., 1973, "Functional Dependence of Torque Coefficient of Coaxial Cylinders on Gap Width and Reynolds Numbers," Journal of Fluids Engineering, 95(1), pp. 122-126.

[18] (IEC), I. E. C., 1999, "Nomencluture for hydroelectric powerplant machinery," IEC/TR 61364.